

Nanoscale

Accepted Manuscript

This article can be cited before page numbers have been issued, to do this please use: K. KUMARANCHIRA RAMANKUTTY, *Nanoscale*, 2024, DOI: 10.1039/D4NR01232A.



This is an Accepted Manuscript, which has been through the Royal Society of Chemistry peer review process and has been accepted for publication.

Accepted Manuscripts are published online shortly after acceptance, before technical editing, formatting and proof reading. Using this free service, authors can make their results available to the community, in citable form, before we publish the edited article. We will replace this Accepted Manuscript with the edited and formatted Advance Article as soon as it is available.

You can find more information about Accepted Manuscripts in the [Information for Authors](#).

Please note that technical editing may introduce minor changes to the text and/or graphics, which may alter content. The journal's standard [Terms & Conditions](#) and the [Ethical guidelines](#) still apply. In no event shall the Royal Society of Chemistry be held responsible for any errors or omissions in this Accepted Manuscript or any consequences arising from the use of any information it contains.

ARTICLE

Circular Dichroism and Circularly Polarized Luminescence of Ligand-protected Molecular Metal Clusters: Insights into Structure-Chiroptical Property Relations

Krishnadas Kumaracnhira Ramankutty*^aReceived 00th January 20xx,
Accepted 00th January 20xx

DOI: 10.1039/x0xx00000x

Molecular noble metal clusters are an emerging class of circularly polarized luminescent (CPL) nanomaterials. Many of the ligand-protected metal clusters exhibit discrete electronic absorption bands which are assigned to their structural components such as metal core, ligands and metal-ligand interfaces. This implies the suitability of CD-CPL approach to unravel structure-chiroptical property relations in molecular metal clusters. Thanks to the tremendous developments in computational methods for investigating the chiroptical properties, along with circular dichroism (CD) and CPL spectroscopy, understanding of the structure-chiroptical properties of these clusters is rapidly progressing. This review discusses various strategies such as the use of chiral ligands, metal atom substitution, ligand exchange, co-crystallization with chiral ligands, *etc.*, for inducing and enhancing the CPL of such metal clusters. This review demonstrates the potential of the combined CD-CPL spectroscopic investigations and theoretical calculations to unravel the origins of photoluminescence and CPL activity of chiral metal clusters.

Introduction

Differential emission of left and right circularly polarized light, known as circularly polarized luminescence (CPL) is one of the most fascinating properties of chiral fluorophores.^[1-2] Small organic molecules, their assemblies,^[3-5] and rare earth metal complexes^[6-7] were the materials of interest in the early years of CPL spectroscopy. CPL from chiral nanomaterials of various dimensions have been reported in the recent past.^[8-13] Among these, atomically precise ligand-protected noble metal clusters are a special class because of their well-defined composition and molecule-like spectroscopic characteristics.^[14-16] Circular dichroism (CD) which is the differential absorption of left- and right-circularly polarized light, and CPL are complementary techniques as they provide insights into the ground state and emissive excited state geometries, respectively, of chiral fluorophores. CD and CPL spectroscopies have been employed extensively to understand the origin of electronic transitions and chirality in small organic molecules.^[17] The molecular characteristics (precise molecular formula, known crystal structures, and discrete electronic absorption bands assignable to distinct structural components) of ligand-protected metal

clusters imply the potential of combined CD-CPL investigations to understand the origin of photoluminescence and chirality in these clusters.^[18] Such investigations are expected to provide structure-chiroptical property relations of these clusters which is one of the important goals in cluster chemistry. Theoretical calculations have also contributed tremendously in this regard. We discuss these aspects taking some of the recently reported CPL-active, ligand-protected noble metal clusters as examples. A better understanding of the structure-chiroptical properties of these clusters could accelerate their use for applications such as anti-counterfeiting, optical displays, *etc.*^[4, 19]

This article also discusses various approaches such as substitution of metal atoms, ligand exchange of achiral ligands with chiral ligands, co-crystallization with chiral ligands, *etc.*, for inducing and enhancing CPL activity in ligand-protected noble metal clusters. The article is structured in the following manner. We first briefly present the basic principles of CD and CPL spectroscopies and define the dissymmetry factors (*g* factors) for absorption (*g_{abs}*) and emission (*g_{lum}*). Then, the complementarity of CD and CPL techniques which enables probing the nature of ground and emissive excited states, respectively, of organic molecules is illustrated with the example of camphor and camphorquinone which are among the thoroughly investigated molecules in chiroptical spectroscopy. The molecular nature of atomically precise noble metal clusters is then briefly explained. Different geometrical origins of chirality in ligand-protected metal clusters are then briefly discussed. Then we discuss some of the reported CPL-active, ligand-protected noble metal clusters in detail. We

^a School of Chemistry, Indian Institute of Science Education and Research
Thiruvananthapuram, Maruthamala P. O., Vithura, Thiruvananthapuram, India,
PIN: 69551

Electronic Supplementary Information (ESI) available: [details of any supplementary information available should be included here]. See DOI: 10.1039/x0xx00000x



compare the signs of the CD bands (especially of the band at the longest wavelength) and the signs of the CPL bands as it is generally performed in case of small organic molecules. The nature of various molecular orbitals (MOs) (as obtained from theoretical calculations), especially those associated with lower energy electronic transitions, are analyzed in terms of the contributions of various atoms in the metal core, metal-ligand

interfaces and in the tail groups of the ligands. This analysis provides insights into the role of distinct structural components on the origin of photoluminescence and chirality in these clusters. Many chiral metal clusters have been reported so far, and there are several review articles and accounts available that summarize the developments in the

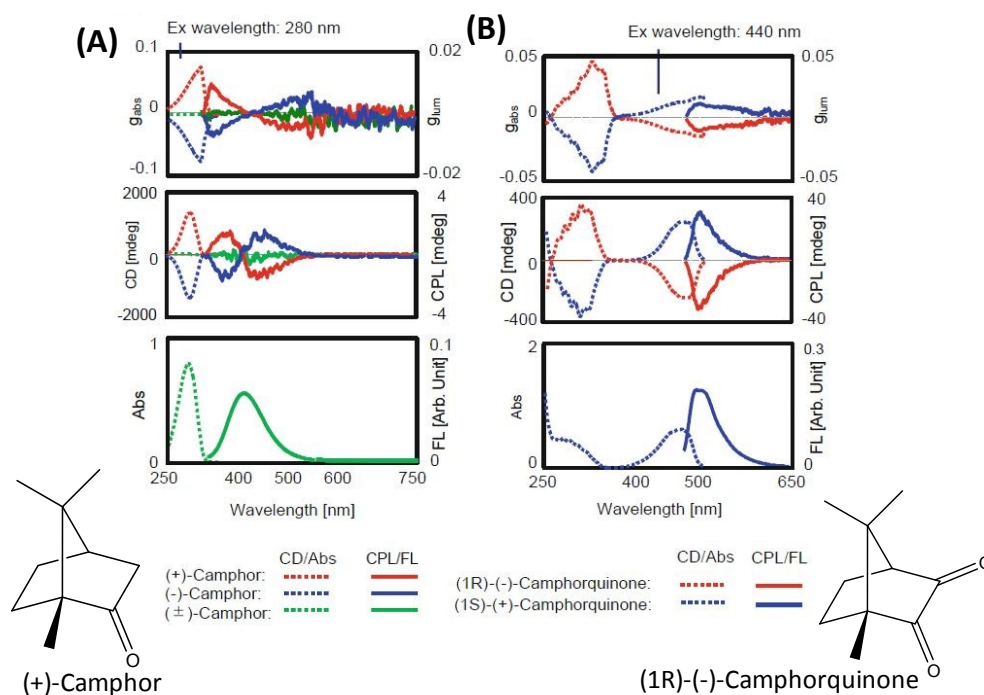


Fig. 1 Experimental CD, CPL, absorption and emission spectra of camphor (A) and camphorquinone (B) (Reproduced from ref. 4 with permission from Springer Nature, Copyright 2020).

chirality^[20-24] and photoluminescence²⁵ of metal clusters in general. This article focuses on the CPL-active ligand-protected noble metal clusters. Though not a noble metal cluster, a Cu_4I_4 -based CPL active material is also discussed because of its interesting circularly polarized thermally activated delayed fluorescence (CP TADF). References to achiral and/or CPL-inactive metal clusters are provided wherever necessary.

Chiroptical Spectroscopy: A brief Introduction

Spectroscopy addresses light-matter interactions of molecules and materials. Chiroptical spectroscopy is a special branch of spectroscopy that deals with the interaction of chiral molecules and materials with polarized light. Two major branches of chiroptical spectroscopy are circular dichroism (CD) and circularly polarized luminescence (CPL).

CD is a special form of electronic absorption (UV/Vis) spectroscopy; in the former, the sample is irradiated alternatively with left- and right-circularly polarized light (CP light) at a particular frequency, and, in the latter, the sample is irradiated with unpolarized light. In CD spectroscopy, a chiral molecule or material absorbs left- and right- CP light to different

extents and this differential absorption left- and right-CP light is referred to as CD. Depending on the wavelength range used, we can have electronic CD (ECD) and vibrational CD (VCD). ECD probes the chirality related to electronic states of molecules while VCD probes the chiral vibrational modes. ECD has been one of the most commonly adopted techniques to probe the secondary structures of proteins, DNA, polymers, *etc.*^[26] VCD is also of immense utility in probing the chiral conformations of biomolecules, peptides, *etc.* A variant of chiroptical spectroscopy that probes vibrational optical activity is Raman Optical Activity (ROA).^[27] Transient CD spectroscopy can be used to understand the chiroptical properties of excited states in molecules.^[28]

Unless otherwise specified, “CD” generally implies ECD, which is the convention followed in this article too. The degree of differential absorption of left and right circularly polarized light (*i.e.*, CD) is quantified using the parameter called dissymmetry factor for absorption (g_{abs}) which is defined as

$$g_{\text{abs}} = 2(\epsilon_L - \epsilon_R) / (\epsilon_L + \epsilon_R) \dots \dots \dots (\text{eq.1})$$

where ϵ_L and ϵ_R are the extinction coefficients for left- and right CP lights, respectively.



Just as CD is a special form of electronic absorption spectroscopy, CPL spectroscopy is a special form of photoluminescence spectroscopy. In conventional photoluminescence spectroscopy, the sample emits unpolarized light *i.e.*, the intensities of left- and right-CP light components are equal in the emitted light. In CPL spectroscopy, a molecule or material will emit right- or left-CP light with different intensities. This differential emission of left- or right-CP light is referred to as CPL. Similarly, the degree of circular polarization in the emitted light (*i.e.*, degree of CPL activity) is

quantified using the parameter called dissymmetry factor for emission or luminescence (g_{lum}) which is defined as

$$g_{lum} = 2(I_L - I_R)/(I_L + I_R) \dots\dots\dots (eq.2)$$

where, I_L and I_R correspond to the intensities of the left- and the right-circularly polarized light, respectively. According to this definition, g_{lum} can have a maximum value of ± 2 .

A chiral molecule or material will exhibit a CD band only if their ground state geometries are chiral. Similarly, a molecule will exhibit CPL activity only if the geometry of the emissive excited state is chiral. Therefore, a combined CD-CPL spectroscopic investigation can

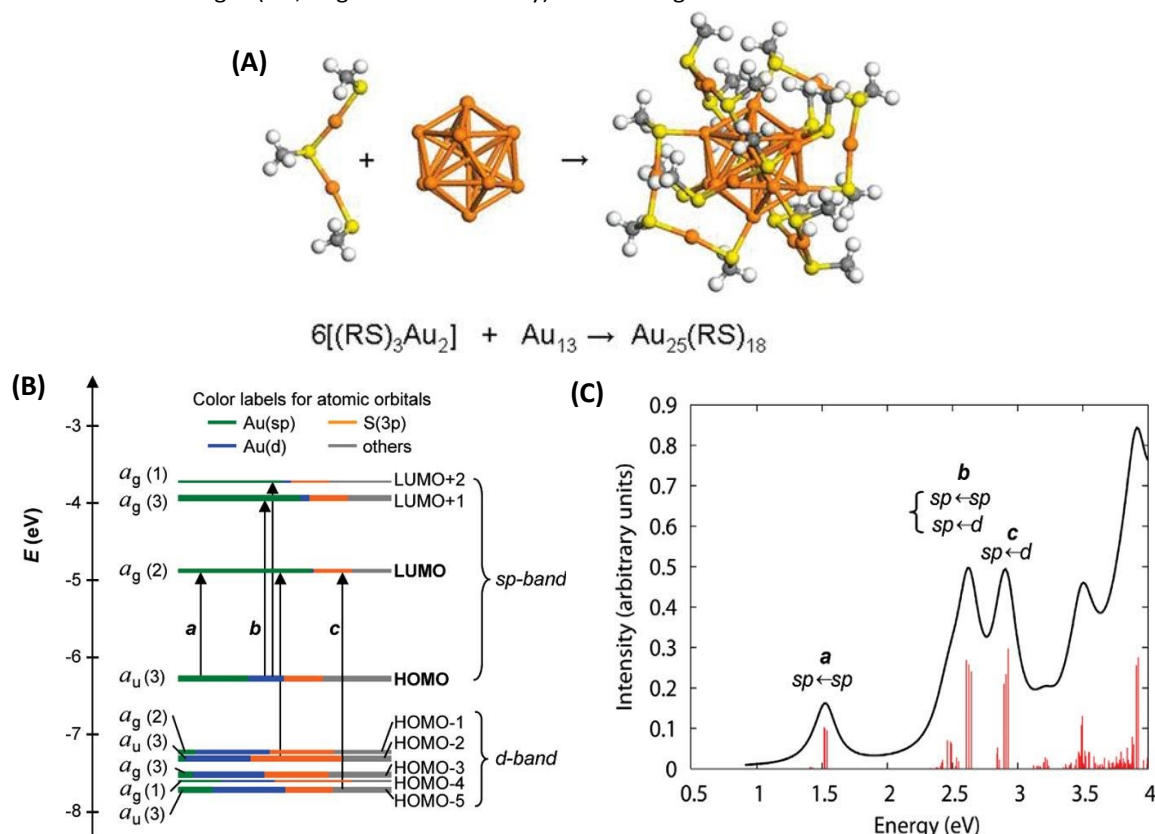


Fig. 2 (A) Schematic of crystal structure of $Au_{25}(SR)_{18}$ (-SR= alkyl/Aryl thiolate) which consists of six $Au_2(SR)_3$ staple motifs protecting an Au_{13} icosahedral core. Color code: Orange (Au) and yellow (S). (B) Kohn-Sham orbital energy level diagram for $Au_{25}(SH)_{18}^-$. The energies are in units of eV. Each KS orbital is drawn to indicate the relative contributions (line length with color labels) of the atomic orbitals of Au (6sp) in green, Au (5d) in blue, S (3p) in yellow, and others in gray (those unspecified atomic orbitals, each with a < 1% contribution). The left column of the KS orbitals shows the orbital symmetry (g, u) and degeneracy (in parenthesis); the right column shows the HOMO and LUMO sets. (C) The theoretical absorption spectrum of $Au_{25}(SH)_{18}^-$. Peak assignments: peak a corresponds to 1.8 eV observed, peak b corresponds to 2.75 eV (observed), and peak c corresponds to 3.1 eV (observed). (Figure 2A is reproduced from ref. 31a with permission from American Chemical Society, Copyright 2008, Figure 2B and 2C are reproduced from ref. 31b with permission from American Chemical Society, Copyright 2008).

provide insights into the structural differences between the geometries of ground and excited states of chiral molecules and materials.

Kasha's rule states photoluminescence occurs, in a large majority of molecules, from the lowest electronic excited states. According to Franck-Condon principle, electronic absorption takes place so fast that the atomic nuclei do not get sufficient time to reorganize. This indicates that molecular geometries of

ground and excited states do not differ significantly. This also implies that the chiroptical properties of the ground and excited states do not differ significantly. As a consequence of the Kasha's rule, in large majority of molecules, CPL spectra consist of a monosignate band with its sign same as that of the CD band



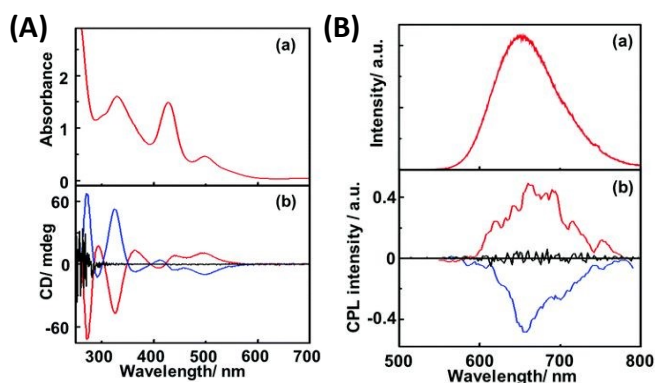


Fig. 3 (A) Absorption (a) and CD spectra (b) of *R*- (red lines), *S*- (blue lines) and *rac*-Ag₂₉(DHLA)₁₂ NCs (black lines) and (B) Emission (a) and CPL spectra (b) of *R*- (red lines), *S*- (blue line) and *rac*-NCs (black line). (Reproduced from ref. 41 with permission from Royal Society of Chemistry, Copyright 2017). DHLA is α -dihydrolipoic acid.

at longest wavelength. This implies that (i) the fluorescence and CPL arise from the same electronic excitation as in the absorption and CD, and that (ii) the geometries (and hence, the relative orientation between electric and magnetic transition dipole moment vectors) of the ground and emissive excited states are not significantly different. A difference in the sign of the CPL and the CD band at the longest wavelength implies a significant structural difference in the geometries of the ground and excited states. Apart from structural differences, the presence of electron withdrawing or donating substituent groups also determines the signs and magnitudes of the CPL bands.^{4, 29} This is because the presence of such groups can alter the electron charge distributions of the chromophore which in turn alter the magnitudes and/or the relative orientations of the electric and magnetic transition dipole moment vectors (see eq. 3 below).

The intensities of the CD and CPL bands are dictated by the quantity called rotational strength or rotatory strength which is, approximately, the product of the magnitudes of the electric (μ) and magnetic (m) transition dipole moment vectors and the angle (θ) between these two vectorial quantities.^[17] An approximate relation between these parameters are given by the equation,

$$R = |\mu| \cdot |m| \cos \theta \dots \dots \dots (\text{eq.3})$$

If these two transition dipole moment vectors are orthogonal ($\theta = 90^\circ$), no CPL activity is observed. The signs and the magnitudes of g_{abs} and g_{lum} values provide insights into the structural differences between ground state and emissive excited state geometries of molecules.^[30, 31]

Illustration of the CD-CPL approach: Examples of Camphor and Camphorquinone

The general principles mentioned above are illustrated with the example of *R*-/*S*-camphor and *R*-/*S*-camphorquinone which are among the most thoroughly studied molecules in chiroptical spectroscopy. Figure 1 presents the superimposed CD and CPL spectra of *R*- and *S*-camphor and *R*-/*S*-camphorquinone. CPL spectra of camphor (Fig. 1A) shows two bands with opposite signs. The sign of the CPL band at longer wavelength is negative while the sign of the longest wavelength CD band is positive. The origin of the two CPL bands with opposite signs and the difference in the signs of CD and CPL bands of camphor is attributed to the presence of two possible excited states with significantly different geometries.³² These two geometries differ in the orientation of the carbonyl group w.r.t. the methylene bridge.³² However, CPL spectrum of camphorquinone (Fig. 1B) shows only one band and its sign is the same as that of the CD band at the longest wavelength. This is attributed to the more rigid structure of camphorquinone (because of the presence of two carbonyl groups) when compared with camphor (which has only one carbonyl group).

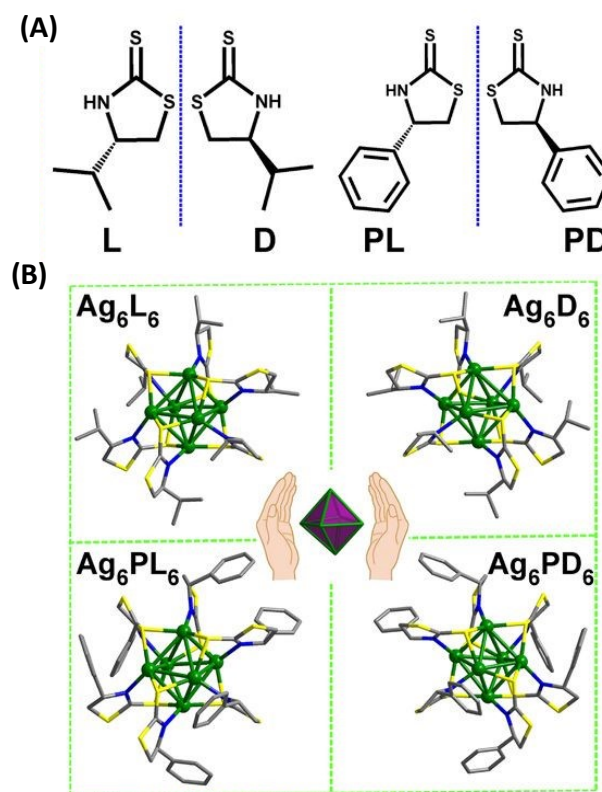


Fig. 4 (A) Structures of (*S*)-/(*R*)-4-isopropylthiazolidine-2-thione (L/D) and (*S*)-/(*R*)-4-phenylthiazolidine-2-thione (PL/PD) ligands. (B) Ball-and-stick representation of the enantiomers of Ag₆L₆/D₆ and Ag₆PL₆/PD₆. Inset: Schematic of the Ag₆ octahedron core in these enantiomers. (Reproduced from ref. 44 with permission from American Association for the Advancement of Science's, Copyright 2020).

The discussion presented above shows that combined CD-CPL approach is promising to unravel the structural differences between the ground- and emissive excited-state geometries of small organic molecules. Now we discuss molecule-like



structural and spectroscopic features of atomically precise, and CPL spectroscopy of such clusters. ligand-protected noble metal clusters before discussing the CD

View Article Online
DOI: 10.1039/D4NR01232A

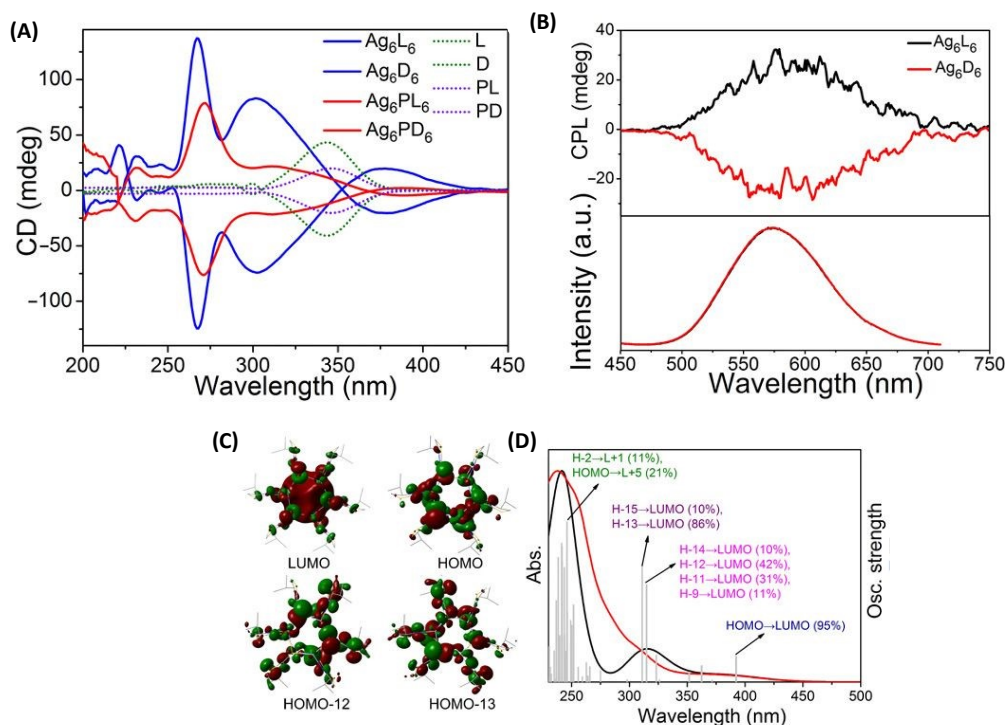


Fig. 5 (A) CD spectra of clusters Ag₆L₆/D₆ and Ag₆PL₆/PD₆, together with ligands L/D and PL/PD in CH₂Cl₂ in the wavelength range of 200 to 450 nm, (B) CPL spectra (top) and the corresponding emission spectra (bottom) of Ag₆L₆ and Ag₆D₆ in CH₂Cl₂. (C) Selected frontier molecular orbital representations for Ag₆L₆ in optimized structures of S₀. (D) Experimental optical absorption spectrum (red) of Ag₆L₆ in CH₂Cl₂ compared to the calculated spectrum (black). Gray bars show the individual transitions (delta function-like peaks showing the relative oscillator strengths). (Reproduced from ref. 44 with permission from American Association for the Advancement of Science's, Copyright 2020).

Molecular characteristics of ligand-protected noble metal clusters

Molecule-like properties of ligand-protected noble metal clusters are well-established using mass spectrometry^[33] and various spectroscopic techniques.^[34] This is illustrated with the example of Au₂₅(SR)₁₈ (SR = alkyl/arylthiolate), one of the most thoroughly studied clusters of this family. Though this cluster is achiral, we chose this example because of its simpler structure compared to other clusters. Au₂₅(SR)₁₈ consists of an Au₁₃ icosahedral core protected by six Au₂(SR)₃ units referred to as staple units as presented in Figure 2A. As shown in Figures 2B and C, discrete electronic absorption bands can be assigned to distinct transitions among various MOs.^{34b} Contribution of various atoms in the icosahedral core, metal-ligand interface and tail groups of ligands to various MOs are also shown in Fig. 2B. It is also shown that the discrete electronic transitions shown in Figure 2B can be assigned as due to transitions localized or delocalized to icosahedral core or the ligands, as shown in Fig. 2C. DFT calculations also have shown that the photoluminescence in Au₂₅(SR)₁₈ is due to transitions localized in the icosahedral core and that involvement of ligands is not significant.^{34b}

Chirality in ligand-protected noble metal clusters

Chirality in metal clusters can arise due to several factors. One of the straightforward ways to induce chirality in metal clusters is to incorporate inherently chiral ligands to achiral metal clusters using ligand exchange strategy.³⁵ Alternatively, metal clusters can be inherently chiral even without the presence of a chiral ligand. Among these, some of the clusters consist of chiral arrangement of achiral ligands on the metal-ligand interfaces.³⁶⁻³⁹ There are also clusters with inherently chiral arrangement of metal atoms in the core.⁴⁰ Further details on the origin of chirality in metal clusters can be found in several review and accounts articles.²⁰⁻²⁴ Specific examples of each of these cases will be discussed in the following sections in the light of their CPL activity.

CPL from ligand-protected noble metal clusters

The first report of CPL from ligand-protected noble metal clusters was by Kumar *et al.*⁴¹ They suggested, based on previous reports, that Ag₂₉(DHLLA)₁₂ (DHLLA = dihydroxy lipoic acid) could be a likely composition for these clusters. The sign of the CPL band was the same as that of the longest wavelength CD band (see Fig. 3), which indicate that the CD and CPL arise from the same electronic transitions. CPL activity of these



clusters was attributed to the chirality in the ligand staples. However, transitions involving the ligands are, in general, expected to occur in the higher energy region, not in the lower energy region. Furthermore, theoretical calculations suggest

that the photoluminescence of this cluster is more likely to be originated from the metal-core centred electronic excitations. Therefore, further experiments are required to confirm the

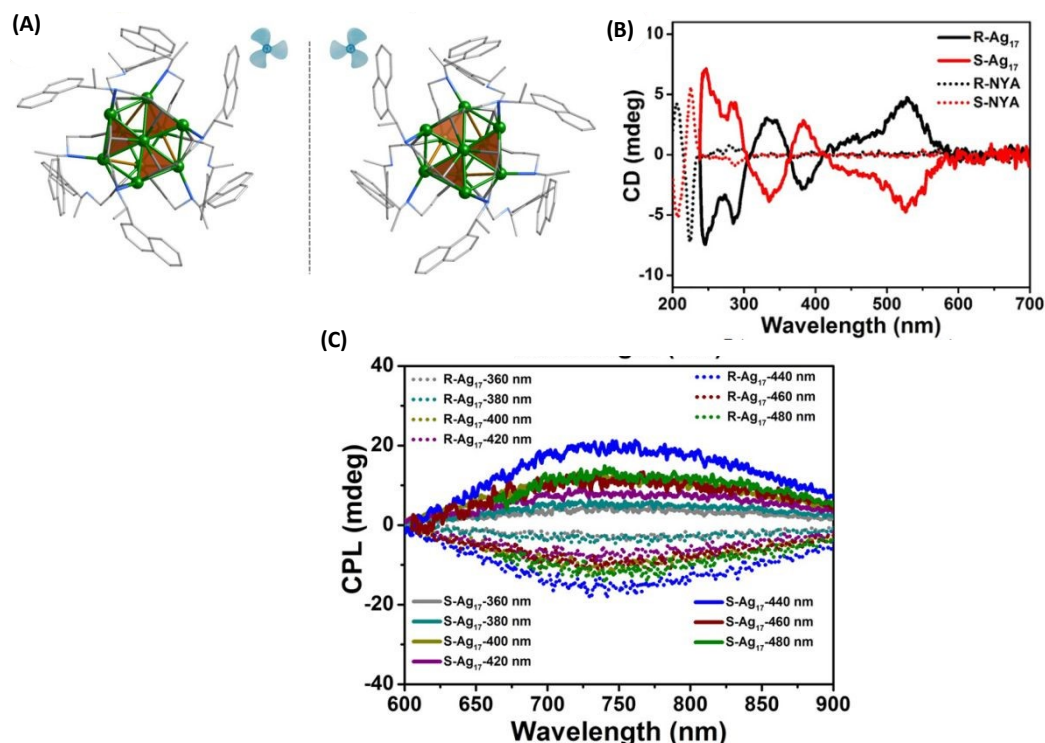


Fig. 6 (A) The aromatic moieties of the ligands resemble a triblade fan when viewed parallel to the C_3 axis. Color code: Ag, green; N, blue; C, gray. All hydrogen atoms have been omitted for clarity. (B), CD spectra of R/S- Ag_{17} (solid trace) and ligands R/S-NYA (dotted trace) in solution and (C) CPL spectra of R/S- Ag_{17} at different excitation wavelengths in the solid state. (Reproduced from ref. 46 with permission from American Chemical Society, Copyright 2021).

origin of CPL activity in Ag_{29} clusters. The observed g_{abs} and g_{lum} values were 1.5×10^{-3} (at 500 nm) and 2×10^{-3} (at 660 nm), respectively. It is worthy to note that the g_{abs} and g_{lum} values are comparable as commonly observed for small organic molecules. This also suggest that the electronic transition corresponding to

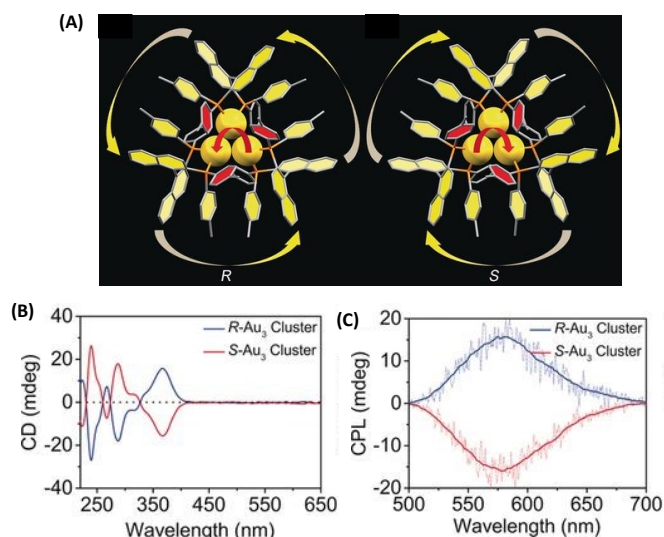


Fig. 7 (A) The overall structures of R/S- Au_3 . Color codes: Au, yellow; P, orange; C, gray (B) CD spectra of $Au_3[(R)\text{-Tol-BINAP}]_3Cl$ and $Au_3[(S)\text{-Tol-BINAP}]_3Cl$ clusters in DCM (C) CPL spectra of R- Au_3 and S- Au_3 assemblies in 70% *n*-hexane. (Reproduced from ref 45 with permission from John Wiley and Sons, Copyright 2017).

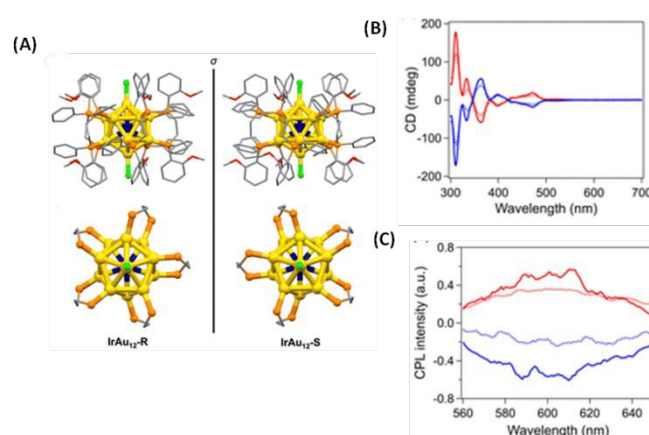


Fig. 8 (A) Crystal structures of $IrAu_{12}\text{-R}$ (left) and $IrAu_{12}\text{-S}$ (right). Phenyl rings, ethylene bridges, and methoxy groups are depicted as sticks and hydrogen atoms are omitted for simplicity, Top view (bottom) of the core structures of $IrAu_{12}\text{-R}$ (left) and $IrAu_{12}\text{-S}$ (right). Phenyl rings and methoxy groups are omitted for simplicity. Color code: yellow, Au; dark blue, Ir;



orange, P; light green, Cl; red, O; gray, C, (B) CD spectra of $\text{IrAu}_{12}\text{-R}$ (red) and $\text{IrAu}_{12}\text{-S}$ (blue) in MeTHF, (C) CPL spectra of $\text{IrAu}_{12}\text{-R}$ (red) and $\text{IrAu}_{12}\text{-S}$ (blue) in MeTHF. (Reproduced from ref. 47 with permission from Royal Society of Chemistry, Copyright 2023).

the CD band at around 500 nm (which correspond to the core-based excitations) might be the transitions responsible for CPL activity in these clusters.
 DOI: 10.1039/D3NR01237A

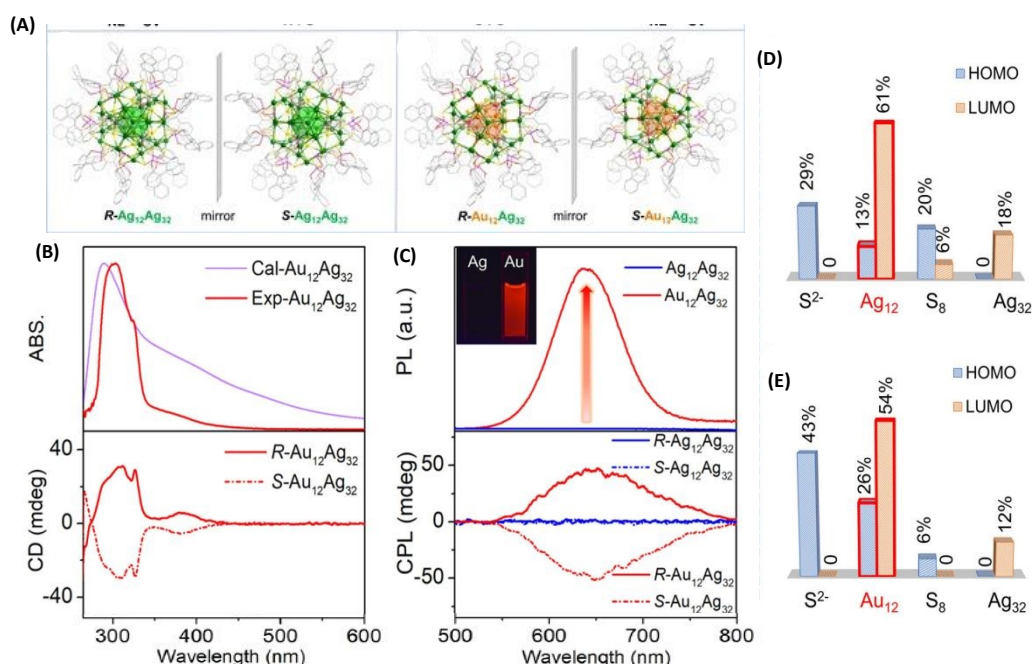


Fig. 9 (A) Ball-and-stick representation of the enantiomers of $R/S\text{-Ag}_{12}\text{Ag}_{32}$ and $R/S\text{-Au}_{12}\text{Ag}_{32}$. For clarity, H atoms are omitted. Color codes for atoms: green, Ag; orange, Au; yellow, S; pink, P; red, O; gray, C. (B) Experimental and calculated absorption (top) and CD spectra (bottom) of $R/S\text{-Au}_{12}\text{Ag}_{32}$ enantiomers in DMAc. (C) Luminescence (top) and CPL spectra (bottom) of $\text{Ag}_{12}\text{Ag}_{32}$ and $\text{Au}_{12}\text{Ag}_{32}$ in DMAc. (D & E) Histograms showing the contributions of different shells and central S^{2-} to the HOMO and LUMO for $\text{Ag}_{12}\text{Ag}_{32}$ and $\text{Au}_{12}\text{Ag}_{32}$ clusters. (Because of the negligible contributions of ligands, they are not listed in this histogram.) (Reproduced from ref. 49 with permission from American Chemical Society, Copyright 2022).

Interestingly, Yoshida *et al.*, has shown that $\text{Ag}_{29}(\text{S}_2\text{R})$ (S_2R = dithiolate ligand) clusters are inherently chiral,⁴² *i.e.*, even in the absence of a chiral ligand such as DHLA. To the best of our knowledge, CPL from these inherently chiral Ag_{29} clusters has not been reported so far (despite the successful separation of their enantiomers).

Han *et al.*, reported strongly CPL-active enantiomers of octahedral $\text{Ag}_6(\text{L}_6/\text{D}_6)$ where L/D correspond to the chiral non-emissive ligand namely, (S)-/(R)-4-isopropylthiazolidine-2-thione (Fig. 4A).⁴⁴ HOMO of these clusters are mostly localized on the Ag, S and N atoms of these clusters while the LUMO is localized on the central Ag atoms. The lowest energy band is attributed mainly to the HOMO-LUMO transitions (see Fig. 5C & D). Therefore, DFT calculations indicate that the CPL activity of these silver clusters originate from ligand-to-metal-metal charge transfer transitions. The observed g_{lum} values were 4.42×10^{-3} . The g_{abs} values were not reported for these clusters. The sign of the CPL band of Ag_6L_6 is the same as that of the CD band at the longest wavelength (Fig. 5A & B). These clusters exhibited exceptionally high quantum yield (QY) of 95 % and photophysical measurements indicate that thermally activated delayed fluorescence (TADF) is responsible for the observed CPL activity and high QY.

Zhang *et al.*, synthesized enantiomeric $[\text{Ag}_{17}(\text{R/S-NYA})_{12}](\text{NO}_3)_3$ (denoted as $R/S\text{-Ag}_{17}$) clusters where $R/S\text{-NYA}$ is $N\text{-}((R/S)\text{-1-(naphthalen-4-yl)ethyl)prop-2-yn-1-amine}$ (Fig. 6A).⁴⁶ The maximum g_{lum} value of $R/S\text{-Ag}_{17}$ at 745 nm was measured to be $\sim \pm 1.2 \times 10^{-3}$. The CPL bands remain almost unchanged when excitation wavelengths were changed from 360 nm to 500 nm, except for slight changes in the intensities as shown in Fig. 6C. DFT calculations indicated that electronic transitions above 300 nm were attributed to the transition between S and P superatomic HOMO and LUMO orbitals. Contributions from the Ag atoms dominates the HOMO (66.4 % Ag, 16.64 % $\text{-C}\equiv\text{C}$ and 7.14 % N) and LUMO (66.85 % Ag, 3.65 % $\text{-C}\equiv\text{C}$ and 22.77 % N) of these clusters while contributions from the $\text{-C}\equiv\text{C}$ groups and N atoms were also considerable. Therefore, electronic transitions responsible for CPL is delocalized across both the ligands and the core Ag atoms. It is worthy to note that the sign of the CD band (at around 538 nm, at the longest wavelength) and the CPL band are opposite (see Fig. 6B and 6C). In general, such a sign change indicates significant structural changes between ground and emissive excited state geometries (see the example of camphor and camphor-quinone discussed earlier). Details of such excited



state changes in geometries have not yet been the focus of current studies on such clusters.

Binaphthalene-based chiral ligands have been extensively used for inducing chiroptical properties to metal clusters.¹⁸ Tang *et al.*, reported CPL activity from three-atom gold cluster, $\text{Au}_3[(R/S)\text{-Tol-BINAP}]_3\text{Cl}$ where $(R/S)\text{-Tol-BINAP}$, (R) - or (S) -2,2'-bis(di-*p*-tolylphosphino)-1,1'-binaphthyl, is a chiral ligand (Fig.

7).⁴⁵ These clusters were soluble in dichloromethane and exhibited distinct CD bands (Fig. 7B), however they did not exhibit any photoluminescence in pure DCM. When hexane was added, these clusters exhibit luminescence and more, interestingly, CPL activity. The maximum g_{lum} observed for these clusters is $\sim 7 \times 10^{-3}$. We note that the signs of the longest wavelength CD band

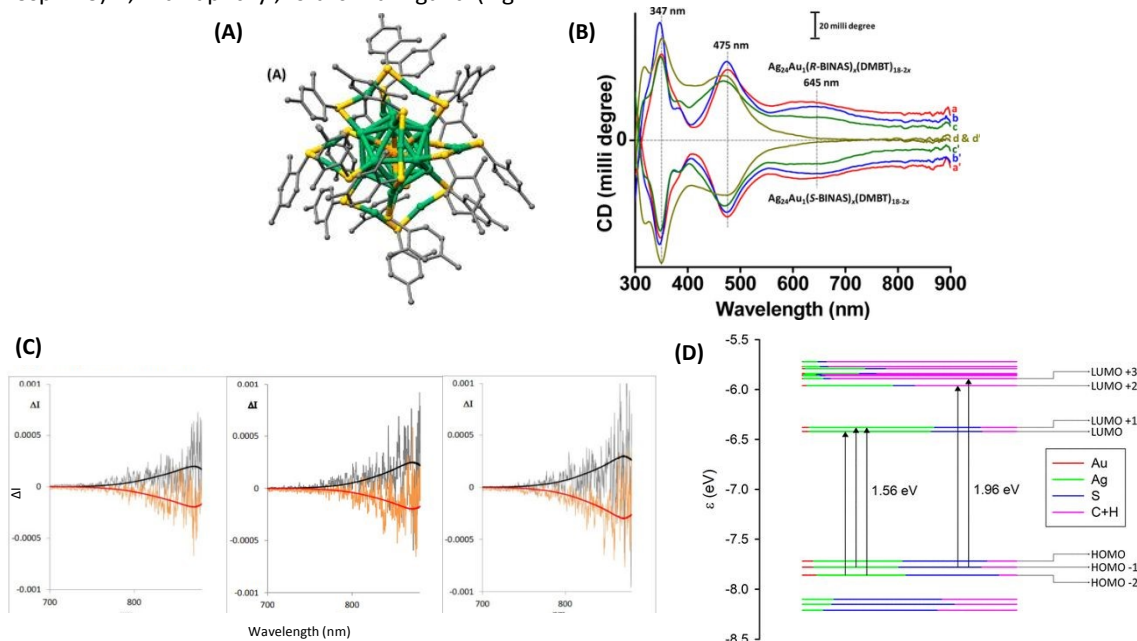


Fig. 10 (A) Schematic of the crystal structure of $\text{Ag}_{24}\text{Au}_1(\text{DMBT})_{18}$. Color codes of atoms in (A): silver (green), gold (orange), sulfur (yellow), and carbon (gray). The H atoms are omitted for clarity. The structure in (A) was created using the coordinates reported in ref 46. (B) CD spectra of $\text{Ag}_{24}\text{Au}_1(R/S\text{-BINAS})_x(\text{DMBT})_{18-2x}$ groups of clusters I (a and a'), II (b and b'), III (c and c'), and IV (d and d'). Traces a–d and a'–d' correspond to the $\text{Ag}_{24}\text{Au}_1(\text{BINAS})_x(\text{DMBT})_{18-2x}$ clusters containing 0–3, 2–5, 3–5 and 4–7 *R*- and *S*-BINAS, respectively. Traces a–c (and a'–c') have been shifted upward (downward) for the sake of clarity. (C) Original CPL spectra of $\text{Ag}_{24}\text{Au}_1(R/S\text{-BINAS})_x(\text{DMBT})_{18-2x}$ group of clusters I (left), II (middle) and III (right). The superimposed black and red traces correspond to the fluorescence spectra recorded on the same instrument: (*R*) black trace, (*S*) red trace. (D) Molecular orbital (energy levels) diagram showing the leading contributions to the two lowest transitions at 1.56 eV (795 nm) and 1.96 eV (632 nm). Orbital character in terms of Mulliken analysis of Ag, Au, S, and C+H contributions is given in terms of colors of the level, according to the inset legend. HOMO and LUMO are at -7.60 and -6.33 eV, respectively. (Reproduced from ref 18 with permission from American Chemical Society, Copyright 2020).

and that of the CPL band are the same (Fig. 7B & C). Emergence of photoluminescence is attributed to the strong C-H... π interactions between the ligands of the clusters in the aggregated form which reduces the non-radiative relaxation pathways. This example demonstrates the importance of solvent effects in understanding the chiroptical properties, especially CPL, of ligand-protected noble metal clusters.

Tsukuda *et al.*, synthesized an enantiomeric pair of superatomic clusters: $[\text{IrAu}_{12}((R,R)\text{-DIPAMP})_5\text{Cl}_2]^+$ and $[\text{IrAu}_{12}((S,S)\text{-DIPAMP})_5\text{Cl}_2]^+$ (referred to as $\text{IrAu}_{12}\text{-}R/S$) where DIPAP is 1,2-bis[(2-methoxyphenyl)phenylphosphino]ethane (See Fig. 8).⁴⁷ This is an interesting system to study the origin of CPL activity because these clusters consist of an symmetric icosahedral IrAu_{12} core and metal atom substitution could be investigated. Single-crystal X-ray diffraction analysis revealed that the icosahedral Ir@Au_{12} core of $\text{IrAu}_{12}\text{-}R/S$ was more twisted along

the Cl–Au–Ir–Au–Cl axis compared with the Au_{13} core of $\text{Au}_{13}\text{-}R/S$, leading to a larger g_{abs} values. The g_{abs} values $\sim 3 \times 10^{-3}$ at 365 nm and $\sim 4 \times 10^{-3}$ at 475 nm, respectively, at 300 K. The $|g_{\text{lum}}|$ values for $\text{IrAu}_{12}\text{-}R/S$ at 300 K were 3×10^{-3} and $\sim 2 \times 10^{-3}$, respectively. Difference in the $|g_{\text{lum}}|$ values between $\text{IrAu}_{12}\text{-}R/S$ were attributed to the limited sensitivity of the CPL spectrometer. The sign of the longest wavelength CD band (at \sim

530 nm) is the same as the CPL band (Fig. 8B and 8C). The magnitudes of the g_{lum} and g_{abs} values were close to each other. DFT calculations suggest that the low energy transitions of this cluster are due to the HOMO-LUMO transitions mostly localized on the IrAu_{12} core⁴⁸ and hence, CPL of these clusters is likely to be originated from core-localized electronic transitions.



Metal atom substitution is known to enhance the emission characteristics of several metal clusters. Along this direction, Mak *et al.*, reported an exciting example of generating CPL by substituting the Ag_{12} core of an $\text{Ag}_{12}\text{Ag}_{32}$ clusters by Au_{12} core (Fig. 9).⁴⁹ The Au-substituted clusters were synthesized using a co-reduction strategy using Ag and Au salts in the synthesis. They employed a chiral ligand, (*R/S*)-binaphthylthiophosphoric acid (abbreviated as *R/S*-PS). The overall symmetry of both cluster systems remained the same because of the high thermodynamic preference for Au atoms to occupy the inner icosahedral sites as presented in Fig. 9A. The resulting $R/S\text{-}[S^{2-}@Ag_{12}@S_8@Ag_{32}(PS)_{24}]^{2+}$ (*R/S*- $\text{Ag}_{12}\text{Ag}_{32}$) clusters did not show any noticeable luminescence (and hence, no CPL) while the $R/S\text{-}[S^{2-}@Au_{12}@S_8@Ag_{32}(PS)_{24}]^{2+}$ (*R/S*- $\text{Au}_{12}\text{Ag}_{32}$) exhibited CPL. The maximum g_{abs} values for *R/S*- $\text{Ag}_{12}\text{Ag}_{32}$ (at 520 nm) and *R/S*- $\text{Au}_{12}\text{Ag}_{32}$ (at 390 nm) was approximately $\pm 3.5 \times 10^{-3}$. The maximum g_{lum} values for *R/S*- $\text{Au}_{12}\text{Ag}_{32}$ was $\sim 6 \times 10^{-3}$. The sign of the longest wavelength CD band (at 390 nm) was the same (positive) as that of the CPL

do not contribute significantly to HOMO and LUMO. These calculations indicate that the CPL is originated from the HOMO-LUMO transitions. This example shows that chiroptical properties such as CPL of ligand-protected metal clusters can be modulated by metal atom substitution.

One of the earliest attempts to employ combined CD-CPL investigations on ligand-protected noble metal clusters was by the author.¹⁸ They aimed to understand the origin of PL in an originally achiral cluster, $\text{Ag}_{24}\text{Au}_1(\text{DMBT})_{18}$ (DMBT = 2,4-dimethyl benzenethiolate). Achiral DMBT ligands were partially exchanged with a chiral bidentate ligand, *R/S*-1,1'-[binaphthalene]-2,2'-dithiol (*R/S*-BINAS) and a series of clusters with mixed ligand composition, $\text{Ag}_{24}\text{Au}_1(\text{R/S-BINAS})_x(\text{DMBT})_{18-2x}$ (x = number of BINAS ligands), were synthesized. These clusters containing 0–3, 2–5, 3–5, and 4–7 BINAS ligands will be referred to as groups I, II, III, and IV, respectively, for convenience. Here we note that the sign (positive) of the CD band at 645 nm

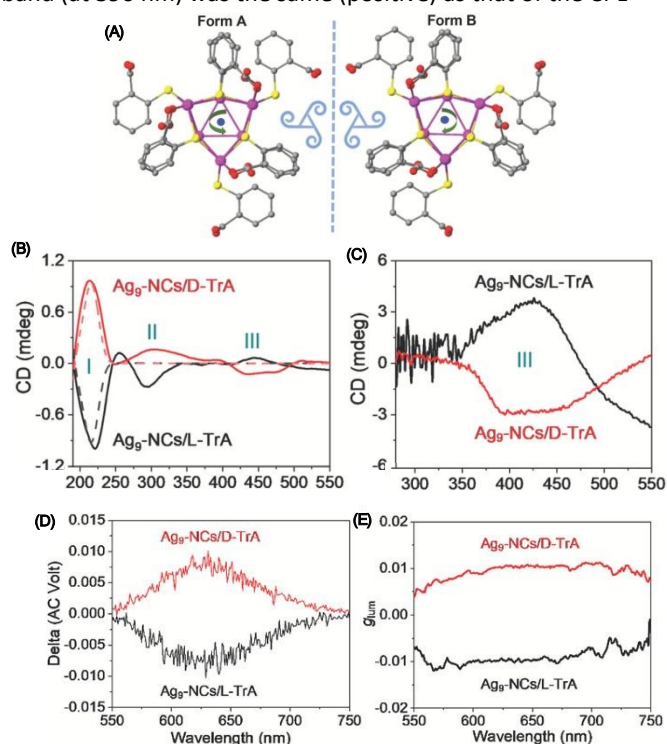


Fig. 11 (A) Top view of $\text{Ag}_9\text{-NCs}$. The peripheral ligands are arranged with a specific direction of rotation, which yields two forms of configuration when viewed from different sides. Insets are drawings of two triskelions. Color labels: purple, Ag; yellow, S; gray, C; red, O. The hydrogen atoms are omitted for clarity. CD spectra of the suspended crystals (B) and dried suspensions (C). The CD spectra of d- and l-TrA (50 mmol L^{-1} in water) are also given (dotted traces in (B)) for comparison. CPL spectra (D) and corresponding g_{lum} factors (E). (Reproduced from ref. 53 with permission from John Wiley and Sons, Copyright 2022).

band (at 626 nm) as shown in Fig. 9B & C. DFT calculations shows that the HOMO of this clusters is mainly localized at the core of $\text{S}^{2-}@M_{12}@S_8$ as presented in Fig. 9D and E. The LUMO spans over the $\text{Au}_{12}/\text{Ag}_{12}$ and Ag_{32} shells. The ligands tail groups

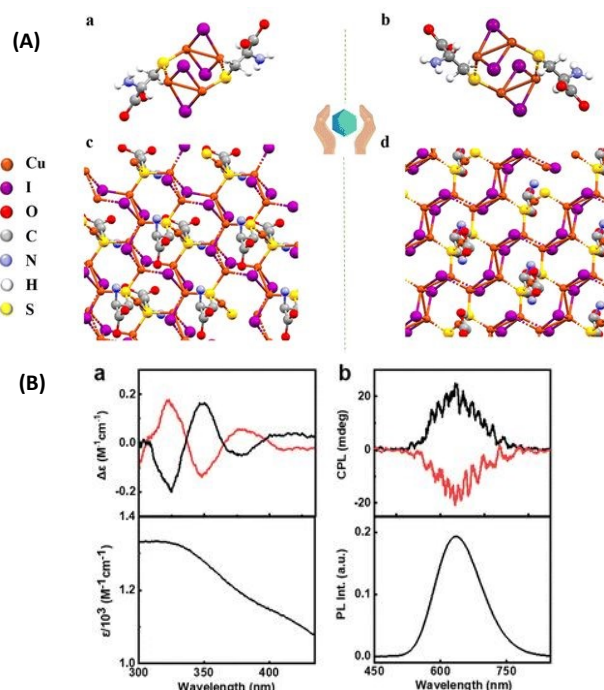


Fig. 12 (A) X-ray crystal structure of (a) (d-Cys) $_2\text{Cu}_4\text{I}_4$ and (b) (l-Cys) $_2\text{Cu}_4\text{I}_4$ nanoclusters and (B) Experimental CD spectra (a) along with the corresponding absorption plot, and experimental CPL spectra (b) along with the corresponding luminescence spectra of the aqueous solution of nanoclusters. Black and red traces correspond to spectra collected from (d-Cys) $_2\text{Cu}_4\text{I}_4$ and (l-Cys) $_2\text{Cu}_4\text{I}_4$ nanoclusters, respectively. (Reproduced from ref. 51 with permission from Royal Society of Chemistry, Copyright 2023).

matches with that of the CPL band (see Fig. 10) According to the DFT calculations, photoluminescence and CPL activity can be assigned to an excitation transfer from the 632 nm band to its neighbouring low-energy excited states (LUMO/LUMO+1) (see Fig. 10D) which should become the leading decay channel in luminescence and CPL. This suggests that the luminescence and CPL activity of $\text{Ag}_{24}\text{Au}_1(\text{R/S-BINAS})_x(\text{DMBT})_{18-2x}$ clusters could



arise from these low-lying excited states (LUMO and LUMO+1) where the contribution of the ligand's tail groups (C and H atoms) is lower compared to that in the higher excited states (LUMO+2 and LUMO+3). The nature of the LUMO and LUMO+1 also explains the low values of CPL, as chiral bands are lost in the evolution of these excited states in which electrons reside in the less chiral $\text{Ag}_{24}\text{Au}_1\text{S}_{18}$ framework of the cluster. As the CD response of the bands predicted at longer wavelengths is very weak, we expect a very low CPL signal, in agreement with experiment. The estimated g_{lum} value was 1.5×10^{-4} . Analysis of the trends in the UV/Vis, CD, luminescence and CPL spectroscopic changes, in conjunction with DFT calculations indicates that the photoluminescence in $\text{Ag}_{24}\text{Au}_1(\text{DMBT})_{18}$ and its chirally functionalized derivatives originate from transitions involving the whole $\text{Ag}_{24}\text{Au}_1\text{S}_{18}$ framework, not merely from the icosahedral $\text{Ag}_{12}\text{Au}_1$ core. Therefore, these results indicate that the photoluminescence in this cluster system cannot be solely attributed to any one of the structural components, such as the metal core or the protecting metal–ligand oligomeric units. This example demonstrates that ligand-exchange strategy can be a promising way to probe the origin of chiroptical properties of metal clusters.

In another approach involving the use of chiral ligands, Feng *et al.*, used D- and L-tartaric acid (TrA) for enhancing the emission and inducing CPL of $\text{Ag}_9(\text{MBA})_9$ (MBA = 2-mercaptobenzoic acid). The emission of $\text{Ag}_9(\text{MBA})_9$ clusters in solution was too weak to be observed at room temperature, however, emission was enhanced after co-crystallization with TrA. Interestingly, the resultant co-crystals exhibited circularly polarized phosphorescence (CPP) (Fig. 11).⁵³ These Ag_9 clusters consists of a core of nine Ag(I) ions as revealed from single crystal X-ray diffraction. These cocrystals showed high g_{lum} values of the order of 10^{-2} . This is one of the highest g_{lum} values reported for a noble metal cluster; typically such clusters exhibit g_{lum} values of the order of 10^{-3} . It is interesting to note that the sign of the CD band at the longest wavelength is negative (for crystals with

D-TrA) while the sign of the CPL band is positive. Theoretical calculations were not available on this system. This work shows that co-crystallization involving chiral molecules could be a potential way to generate CPL from metal clusters.

It is interesting to note that the CD spectra measured for the suspended crystals and dried crystals are dramatically different (see Fig. 11). Three distinct CD bands were observed for the suspension while only one band was observed for the dried crystals. Reasons for this difference is unclear, however, the possibility of scattering effects (which will worsen at longer wavelengths) and solvent induced changes were suggested. The CD band III for suspension is retained (with significantly higher intensities) even after drying and the signs of this band was also preserved. Linear polarization artefacts (which is one of the most common artefact in CPL spectroscopy) were ruled out by measuring linear dichroism (LD) measurements. However, it is unclear from their description whether these measurements are performed in a suspension or in the dried form. This is important to be clarified especially because the reported CPL spectra correspond to the vacuum dried crystals.

Kumar *et al.*, synthesized enantiomeric Cu_4I_4 clusters (Fig. 12) protected with a chiral ligand D/L-Cysteine.⁵¹ Thin films of these clusters CPL activities with a significantly high g_{lum} values of 1.22×10^{-2} which is an order of magnitude higher than other nanomaterials with chiral emission. The sign of the longest wavelength CD band was the same as that of the CPL band indicating that the CPL is originating from the same electronic transition (Fig. 12B). In order to test the linear polarization artefacts in CPL measurements of thin films, the films were rotated and flipped along different angles and no significant changes in g_{lum} values or signs were observed, which indicate the absence of such artefacts. Chen *et al.*, also reported a similar CPL-active Cu_4I_4 system consisting of a chiral ligand, namely, R/S-3-quinuclidinol.⁵²

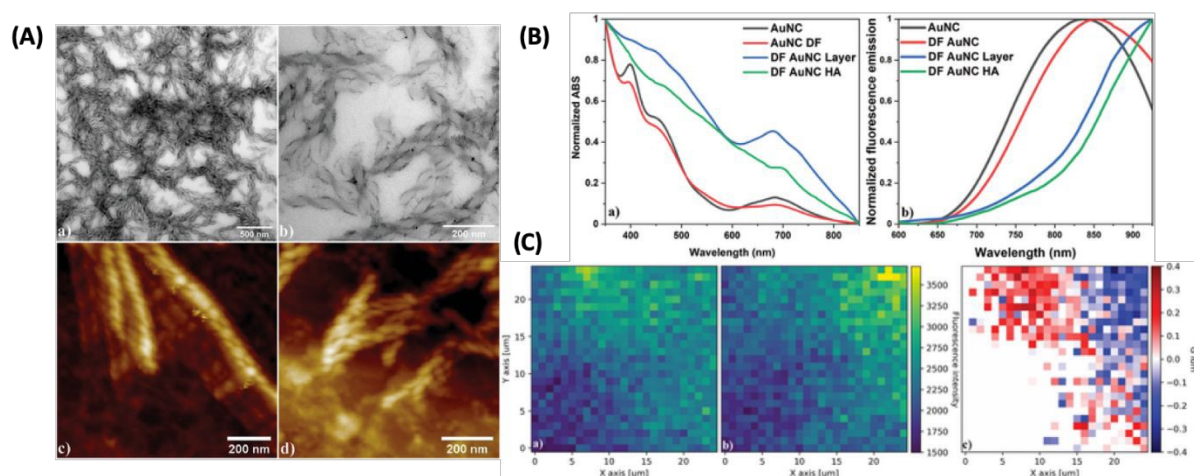


Fig. 13 (A) Liquid crystalline OIM helical nanofilaments coated with double-functionalized gold nanoclusters (DF AuNC HA) made using liquid crystal template imaged under: a,b) TEM and AFM domains with: c) left-handed and d) right-handed nanofilaments



are distinguished, (B) Comparison of: a) normalized absorption and b) fluorescence emission spectra between unfunctionalized (AuNC) and double-functionalized Au₂₅PET₁₈ nanoclusters (DF AuNC) measured from solutions, dry layers, and helical assemblies (HA). Dry layers of AuNCs (DF AuNC) were prepared in the same manner (heating/cooling procedure) as helical assemblies, but without the OIM template, (C) 2D maps showing a) left-handed and b) right-handed circularly polarized luminescence measured from sample with helical assemblies of gold nanoclusters (DF AuNC HA) along with: c) g_{lum} calculated for this set of data. Both CPL maps are drawn using the same fluorescence intensity scale. (Reproduced from ref. 54 with permission from John Wiley and Sons, Copyright 2022).

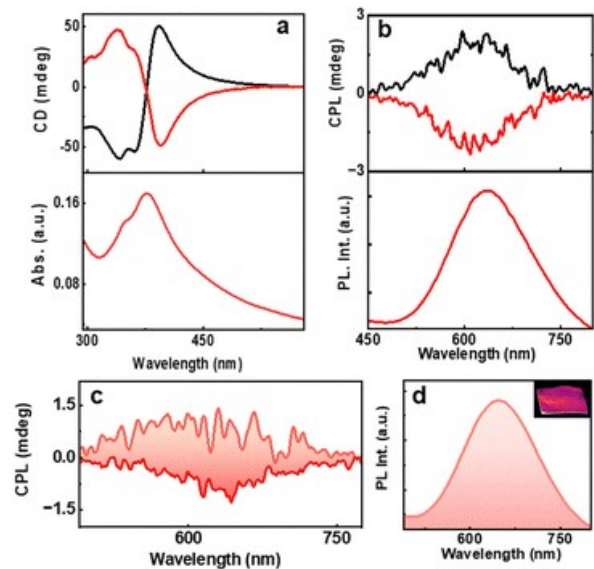


Fig. 14 (a) CD and the corresponding UV-visible spectra and (b) CPL and the corresponding PL spectra of aqueous AuNC solution. Black and red traces correspond to D- and L-AuNCs, respectively. (c) CPL and the (d) luminescence plot of the AuNC incorporated PVA film. The positive and negative CPL plot corresponds to D- and L-AuNC, respectively. The inset in 'd' shows the photograph of the film under 365 nm UV illumination. (Reproduced from ref. 55 with permission from Royal Society of Chemistry, Copyright 2023).

One of the ways to induce or enhance the CPL activity is to use a template or a matrix material that can interact with the chiral fluorophore. Lipok *et al.*, used such a strategy wherein a liquid-crystal-like ligand (4-[(16-sulfanylhexadecanoyl)oxy]phenoxy-4-(hexadecyloxy)benzoate) for imparting chirality to an achiral cluster, namely, Au₂₅(PET)₁₈ where PET is 2-phenylethanethiolate as shown in Fig. 13.⁵⁴ CPL from these clusters with high g_{lum} values reaching maximally 0.32 and -0.37 for the domains of opposite handedness were observed. This is arguably the highest g_{lum} value reported for a noble metal cluster reported so far. This is a surprising result because the PL efficiency of Au₂₅(PET)₁₈ is inherently low. This example shows the promising use of matrices or templates for generating CPL-activity from relatively weakly fluorescent or even achiral metal clusters.

Kumar *et al.*, also reported a six-atom gold cluster/complex, [Au₆(D-/L-Cys)₈]²⁺ where D-/L-Cys are enantiomers of Cysteine which is used as a chiral protecting ligand (Fig. 14).⁵⁵ These clusters exhibited dual photoemission (fluorescence and phosphorescence). Interestingly, phosphorescence showed circularly polarization. The estimated g_{lum} values for D-AuNCs/L-AuNCs were -8.1×10^{-3} / $+6.2 \times 10^{-3}$. The signs of the first CD band and the CPL band were the same, indicating the similar excited state structure involved in the absorption and emission.

Cluster	Ligand (Chiral/Achiral)	$ g_{lum} $ (λ_{max})	CPL detected in solution/solid state	Ref.
Ag ₂₉ (DHLLA) ₁₂	Dihydroxyloipoic acid (chiral)	2×10^{-3} (660 nm)	Solution	Ref. 41
Ag ₆ (L ₆ /D ₆) (L/D = Ligands)	(S)-/(R)-4-isopropylthiazolidine-2-thione (chiral)	4.42×10^{-3} (574 nm)		Ref. 44
[Ag ₁₇ (R/S-NYA) ₁₂](NO ₃) ₃ (NYA = Ligand)	N-((R/S)-1-(naphthalen-4-yl)ethyl)prop-2-yn-1-amine (chiral)	1.2×10^{-3} (745 nm)	Solution	Ref. 46
Au ₃ [(R/S)-Tol-BINAP] ₃ Cl	(R)- or (S)-2,2'-bis(di- <i>p</i> -tolylphosphino)-1,1'-binaphthyl (chiral)	7×10^{-3} (583 nm)	Solution	Ref. 45
[IrAu ₁₂ ((R,R)/(S,S)-DIPAMP) ₅ Cl ₂] ⁺	1,2-bis[(2-methoxyphenyl)phenylphosphino]ethane (chiral)	3×10^{-3} (600 nm)	Solution	Ref. 47
[Au ₁₃ ((R,R)-DIPAMP) ₅ Cl ₂] ³⁺	1,2-bis[(2-methoxyphenyl)phenylphosphino]ethane (chiral)	2×10^{-3} (760 nm)	Solution	Ref. 48
R/S-[S ²⁻ @Ag ₁₂ @S ₈ @Ag ₃₂ (PS) ₂₄] ²⁺	(R/S)-binaphthylthiophosphoric acid (chiral)	6×10^{-3} (626 nm)	Solution	Ref. 49

$\text{Ag}_{24}\text{Au}_1(\text{R/S-BINAS})_x(\text{DMBT})_{18-2x}$	R/S-1,1'-[binaph-thalene]-2,2'-dithiol (chiral)	1.5×10^{-4} (880 nm)	Solution	Ref. 18
$\text{Ag}_9(\text{MBA})_9$	MBA = 2-mercaptobenzoic acid (achiral)	1.05×10^{-2} (630 nm)	Crystals	Ref. 53
$(\text{d/l-Cys})_2\text{Cu}_4\text{I}_4$	D/L-Cysteine (chiral)	1.22×10^{-2} (625 nm)	Solution	Ref. 51
$\text{Au}_{25}(\text{PET})_{18}$	PET = 2-Phenylethanethiol (achiral)	0.32 (880 nm)	Films	Ref. 54
$[\text{Au}_6(\text{D-/L-Cys})_8]^{2+}$	D/L-Cysteine (chiral)	8.1×10^{-3} (625 nm)	Solution	Ref. 55
$[\text{Cu}_3(\text{R/S-NHCpy})_3]_2(\text{PF}_6)_6 \cdot (\text{CH}_3\text{CN})_{7.5}$	R/S-NHCpy-H-PF ₆ (chiral)	2.1×10^{-3} (455 nm)	Solution	Ref. 56
$[\text{Cu}_{15}\text{Ag}_4(\text{R/S-PEA})_{12}](\text{BF}_4)_5$	N-((R/S)-1-phenylethyl)prop-2-yn-1-amine (chiral)	1×10^{-3} (608 nm)	Crystals	Ref. 57
$\text{R/S-(Cu}_6(\text{ippt})_6)$	R/S-4-isopropylthiazolidine-2-thione (chiral)	Not reported, (858 nm)	Solid state	Ref. 58
$\text{Au}_5(\text{MPA})_5$	MPA= mercaptopropionic acid (with Zn^{2+} ion and Tween-20- a chiral surfactant)	13×10^{-3} (443 nm)	Solution	Ref. 59
AuAg@AMP (exact composition not known)	AMP = Adenosine 5'-monophosphate (ligand), G-quadruplex (chiral template)	1.3×10^{-2} 9 (for L-clusters) and 2.7×10^{-2} (for R-clusters) (475 nm)	Solution	Ref. 60
$\text{Cu}_2\text{I}_2(\text{BINAP})_2$	R/S-BINAP: (R/S)-2,2'-bis(diphenylphosphino)-1,1'-binaphthalene (chiral)	9.5×10^{-3} (543 nm)	Microcrystals dispersed in ethanol	Ref. 61
$\text{Cu}_4\text{I}_4(\text{R/S-3-quinuclidinol})_3$	R/S-3-quinuclidinol (chiral)	4.3×10^{-3} (for R) and 4.1×10^{-3} (for S) (580 nm)	Powdered crystals	Ref. 62

Table 1: CPL-active, ligand-protected metal clusters reported so far and their key chiroptical properties.

A summary of the CPL-active, ligand-protected metal clusters and their key properties are presented in Table 1. The table shows that g_{lum} values of most of the clusters were of the order of 10^{-3} which is comparable to small organic fluorophores: some of them exhibited g_{lum} values an order of magnitude higher as well.

CD, CPL and DFT studies on ligand-protected, atomically precise metal clusters presented above reveal that CPL activity in some of the clusters arise out of the core-localized electronic transitions whereas CPL activity in some other clusters arise out of the electronic transitions that are delocalized across metal-ligand interface. The use of inherently chiral ligands seems to be the most common strategy for inducing chirality to the clusters and to induce CPL-activity in metal clusters. Ligand exchange of clusters (consisting of achiral ligands) with chiral ligands have also been employed for inducing CPL-activity in such clusters. These examples raise the following questions: Is the chiral ligand/template necessary for such clusters to exhibit CPL activity? Can an inherently chiral metal cluster (*i.e.*, clusters without any chiral ligands or chiral templates) in solution exhibit CPL activity? Clusters such as Ag_{29} and Au_{38} , *etc.*, could be suitable candidates for such studies. Effects of electron-donating or withdrawing substituents are also to be probed in order to have better clues for enhancing the CPL activity in these clusters.

Conclusions

This article highlights the importance of chiroptical spectroscopy in understanding the structure-chiroptical property relations of atomically precise, ligand-protected metal clusters. We mainly focus on the CD and CPL spectroscopy and theoretical simulations to unravel the origins of chirality and photoluminescence in these clusters. The article also provides a timely account of the emergence of atomically precise, ligand-protected noble metal clusters as a new class of CPL-active nanoscale fluorophores.

Compared to organic molecules, analysis of emissive excited state geometries is challenging for these clusters owing to their larger sizes and resulting complex electronic structure and higher computational costs. Many of these clusters exhibit g_{lum} values of the order of 10^{-3} which is comparable to organic molecules and several other CPL-active nanoscale fluorophores. Some of the clusters discussed here exhibit considerable CPL-activity in the self-assembled form or in a matrix-embedded form which is promising in the context of CPL-related applications. However, there is a need to develop better methods to pattern these CPL-active clusters in order to make use of the CPL-activity of these clusters for applications.

Chiroptical measurements of such clusters should be conducted more thoroughly and rigorously in order to test for potential artefacts, and one has to clearly report the control experiments. This is especially important for CPL measurements. Relatively less explored techniques such as VCD, ROA are expected to be employed to greater extents to investigate ligand-protected metal clusters. Efforts towards cluster-assembled materials



when combined with chiroptical measurements could create potential materials for chirality-based applications. Another important aspect when considering the chirality of these clusters is their inherent dynamics of their cores as well as their metal-ligand interfaces. Understanding the roles of these aspects could lead to designing metal clusters with enhanced chiroptical properties. We hope that our article will accelerate the research activities in the chiroptical activity of metal clusters and nanomaterials in general, toward better understanding their structure-property relationships.

Conflicts of interest

There are no conflicts to declare.

Acknowledgements

K. R. K. gratefully acknowledge the Science and Engineering Research Board, Govt. of India for the Ramanujan Fellowship (Grant No: RJF/2022/000022). K. R. K. also acknowledge the financial and other means of support from the Indian Institute of Science Education and Research Thiruvananthapuram, India. K. R. K. gratefully acknowledge the constant support of Dr. Reji Varghese in terms of insightful discussions and for providing the laboratory facilities.

References

- J. P. Riehl, F. Richardson, *Chem. Rev.*, 1986, **86**, 1, 1–16.
- J. P. Riehl, F. Richardson, *Chem. Rev.* 1977, **77**, 6, 773–792.
- J. Kumar, T. Nakashima, T. Kawai, *J. Phys. Chem. Lett.*, 2015, **6**, 3445–3452.
- Circularly Polarized Luminescence of Isolated Small Organic Molecules, Ed. By T. Mori, Springer Publications, 2020.
- C. K. Luk, F. S. Richardson, *J. Am. Chem. Soc.*, 1974, **96**, 2006–2009.
- F. Zinna, L. di Bari, *Chirality*, 2015, **27**, 1–13.
- Y. Zhong, Z. Wu, Y. Zhang, B. Dong, X. Bai, *InfoMat.*, 2023, **5**, e12392.
- J. George, K. G. Thomas, *J. Am. Chem. Soc.*, 2010, **132**, 2502–2503.
- M. Golla, S. K. Albert, S. Atchimnaidu, D. Perumal, N. Krishnan, R. Verghese, *Angew. Chem. Int. Ed.*, 2019, **58**, 3865–3869.
- R. Dhall, K. Seyler, Z. Li, D. Wickramaratne, M. R. Neupane, I. Chatzakis, E. Kosmowska, R. K. Lake, X. Xu, S. B. Cronin, *ACS Photonics*, 2016, **3**, 310–314.
- U. Tohgha, K. K. Deol, A. G. Porter, S. G. Bartko, J. K. Choi, B. M. Leonard, K. Varga, J. Kubelka, G. Muller, M. Bala, *ACS Nano*, 2013, **7**, 11094–11102.
- M. Sujith, E. K. Vishnu, S. Sappati, M. S. O. Hassan, V. Vijayan, K. G. Thomas, *J. Am. Chem. Soc.*, 2022, **144**, 5074–5086.
- S. D. Noja, F. Amato, F. Zinna, L. D. Bari, G. Ragazzon, M. Prato, *Angew. Chem. Int. Ed.*, 2022, **134**, e202202.
- I. Chakraborty, T. Pradeep, *Chem. Rev.*, 2017, **117**, 8208–827.
- R. Jin, C. Zeng, M. Zhou, Y. Chen, *Chem. Rev.*, 2016, **116**, 10346–10413.
- H. Hakkinen, *Nat. Chem.*, 2012, **4**, 443–455.
- G. Longhi, E. Castiglioni, J. Koshoubu, G. Mazzeo, S. Abbate, *Chirality*, 2016, **28**, 696–707.
- K. R. Krishnadas, L. Sementa, M. Medves, A. Fortunelli, M. Stener, A. Furttsenberg, G. Longhi, T. Bürgi, *ACS Nano*, 2020, **14**, 9687.
- (a) J. V. Rival, P. Maimoona, R. Vinoth, A. M. V. Mohan, E. S. Shibu, *ACS Appl. Mater. Interf.*, 2021, **13**, 10583–10593. (b) M. P. Duffy, W. Delaunay, P.-A. Douit, M. Hissler, *Chem. Soc. Rev.*, 2016, **45**, 5296–5310.
- Y. Zhu, J. Guo, X. Qiu, S. Zhao, Z. Tang, *Acc. Mater. Res.*, 2021, **2**, 21–35.
- S. Knoppe, T. Bürgi, *Acc. Chem. Res.*, 2014, **47**, 1318–1326.
- J.-H. Huang, X.-Y. Dong, Y.-J. Wang, S.-Q. Zang, *Coord. Chem. Rev.*, 2022, **470**, 214729.
- Y. Zhu, J. Guo, X. Qiu, S. Zhao, Z. Tang, *Acc. Mater. Res.*, 2021, **2**, 21–35.
- B.-W. Zhou, S. Zhang, L. Zhao, *Mater. Chem. Front.*, 2023, **7**, 6389–6410.
- M.-M. Zhang, K. Li, S.-Q. Zhang, *Adv. Opt. Mater.*, 2022, **8**, 1902152.
- Comprehensive Chiroptical Spectroscopy, Vol. I and II*, Ed. N. Berova, P. L. Polavarapu, K. Nakamishi, R. W. Woody, Wiley & Sons Inc.
- Chiroptical Spectroscopy: Fundamentals and Applications*, P. L. Polavarapu, CRC Press, Taylor and Francis Group.
- (a) J. W. Lewis, R. F. Tilton, C. M. Einterz, S. J. Milder, I. D. Kuntz, D. S. Kliger, *J. Phys. Chem.*, 1985, **89**, 289–204. (b) M. Schmid, L. Martinez-Fernandez, D. Markovitsi, F. Santoro, F. Hache, R. Improt, P. Changenet, *J. Phys. Chem. Lett.*, 2019, **10**, 4089–4094. (c) J. Meyer-Ilse, D. Akimov, B. Dietzek, *Laser & Photon. Rev.* 2013, **7**, 495–505.
- Z. Dominguez, R. Lopez-Rodriguez, E. Alvarez, S. Abbate, G. Longhi, U. Pischel, A. Ros, *Chem. Eur. J.*, 2018, **24**, 12660–12668.
- H. Tanaka, Y. Inoue, T. Mori, *Chem. Photo. Chem.*, 2018, **2**, 386–402.
- S. Thi, Duong and M. Fujiki, *Polym. Chem.*, 2017, **8**, 4673.
- G. Longhi, E. Castiglioni, S. Abbate, F. Lebon, D. A. Lightner, *Chirality*, 2013, **25**, 589–599.
- R. L. Whetten, J. T. Khoury, M. M. Alvarez, S. Murthy, I. Vezmar, Z. L. Wang, P. W. Stephens, C. L. Cleveland, W. D. Luedtke, U. Landman, *Adv. Mater.*, 1996, **8**, 428–433.
- (a) J. Akola, M. Walter, R. L. Whetten, H. Hakkinen H. Gronbeck, *J. Am. Chem. Soc.*, 2008, **130**, 3756–3757. (b) M. Zhu, C. M. Aikens, F. J. Hollander, G. C. Schatz, R. Jin, *J. Am. Chem. Soc.*, 2008, **130**, 5883–5885.
- T. G. Schaaff, R. L. Whetten, *J. Phys. Chem. B*, 2000, **104**, 2630–2641.
- P. D. Jadzinsky, G. Calero, C. J. Ackerson, D. A. Bushnell, R. D. Kornberg, *Science*, 2007, **318**, 430.
- I. Dolamic, S. Knoppe, A. Dass, T. Bürgi, *Nat. Commun.*, 2012, **3**, 798.
- S. Knoppe, I. Dolamic, A. Dass, T. Bürgi, *Angew. Chem. Int. Ed.*, 2012, **51**, 7589–7591.
- H. Qian, W. T. Eckenhoff, Y. Zhu, T. Pintauer, R. Jin, *J. Am. Chem. Soc.*, 2010, **132**, 8280–8281.
- X.-K. Wan, S.-F. Yuan, Z.-W. Lin, Q.-M. Wang, *Angew. Chem. Int. Ed.*, 2014, **53**, 2923–2926.
- J. Kumar, T. Kawai, T. Nakashima, *Chem. Commun.*, 2017, **53**, 1269–1272.
- H. Yoshida, M. Ehara, U. D. Priyakumar, T. Kawai, T. Nakashima, *Chem. Sci.*, 2020, **11**, 2394–2400.
- Y. Zeng, S. Havenridge, M. Gharib, A. Baksi, K. L. D. M. Weerawardene, A. R. Ziefuß, C. Strelow, C. Rehbock, A. Mews, S. Barcikowski, M. M. Kappes, W. J. Parak, C. M. Aikens, I. Chakraborty, *J. Am. Chem. Soc.*, 2021, **143**, 9405–9414.
- Z. Han, X.-Y. Dong, P. Luo, S. Li, Z.-Y. Wang, S.-Q. Zang, T. C. W. Mak, *Sci. Adv.*, 2020, **6**, eaay0107.



- 45 L. Shi, L. Zhu, J. Guo, L. Zhang, Y. Shi, Y. Zhang, K. Hou, Y. Zheng, Y. Zhu, J. Lv, S. Liu, Z. Tang, *Angew. Chem. Int. Ed.*, 2017, **56**, 15397-15401.
- 46 M.-M. Zhang, X.-Y. Dong, Z.-Y. Wang, X.-M. Luo, J.-H. Huang, S.-Q. Zhang, T. C. W. Mak, *J. Am. Chem. Soc.*, 2021, **143**, 6048-6053.
- 47 H. Hirai, T. Nakashima, S. Takano, Y. Shichibu, K. Konishi, T. Kawai, T. Tsukuda, *J. Mater. Chem. C*, 2023, **11**, 3095-3100.
- 48 H. Hirai, S. Takano, T. Nakashima, T. Iwasha, T. Taketsugu, T. Tsukuda, *Angew. Chem. Int. Ed.*, 2022, **61**, e202207290.
- 49 Y.-J. Kong, J.-H. Hu, X.-Y. Dong, Y. Si, Z.-Y. Wang, X.-M. Luo, H.-R. Li, Z. Chen, S.-Q. Zhang, T. C. W. Mak, *J. Am. Chem. Soc.*, 2022, **144**, 19739-19747.
- 50 M. S. Bootharaju, C. P. Joshi, M. R. Parida, O. F. Mohammed, O. M. Bakr, *Angew. Chem. Int. Ed.*, 2016, **55**, 922-926.
- 51 C. Dutta, S. Maniappan, J. Kumar, *Chem. Sci.*, 2023, **14**, 5593-5601.
- 52 J. Chen, X. Pan, X. Zhang, C. Sun, C. Chen, X. Ji, R. Chen, L. Mao, *Small*, 2023, **19**, 2300938.
- 53 N. Feng, Z. Wang, D. Sun, P. Sun, X. Xin, X. Cheng, H. Li, *Adv. Optica Mater.*, 2022, **10**, 2102319.
- 54 M. Lipok, P. Obstarczyk, S. Parzyszek, Y. Wang, M. Bagiński, T. Buerger, W. Lewandowski, J. Olesiak-Bañska, *Adv. Optical Mater.*, 2023, **11**, 2201984.
- 55 C. Dutta, S. Maniappan, J. Kumar, *Chem. Comm.* 2023, **59**, 13735-13738.
- 56 X.-H. Ma, Y. Si, J.-H. Hu, X.-Y. Dong, G. Xie, F. Pan, Y.-L. Wei, S.-Q. Zhang, Y. Zhao, *J. Am. Chem. Soc.*, 2023, **145**, 25874-25886.
- 57 M. M. Zhang, K.-K. Gao, X.-Y. Dong, Y. Si, T. Jia, Z. Han, S.-Q. Zhang, T. C. W. Mak, *J. Am. Chem. Soc.*, 2023, **145**, 22310-22316.
- 58 Z. Han, Y. Si, X.-Y. Dong, J.-H. Hu, C. Zhang, X.-H. Zhao, J.-W. Yuan, Y. Wang, S.-Q. Zhang, *J. Am. Chem. Soc.*, 2023, **145**, 6166-6176.
- 59 S. Basu, M. P. Bakulic, Z. S. Marcic, V. Bonacic-Koutecky, N. Ambursky, *ACS Nano*, 2023, **17**, 16644-16655.
- 60 Z. Suo, X. Hou, J. Chen, X. Liu, Y. Liu, F. Xing, Y. Chen, L. Feng, *J. Phys. Chem. C*, 2020, **124**, 21094-21102.
- 61 J.-J. Wang, H.-T. Zhou, J.-N. Yang, L.-Z. Feng, J.-S. Yao, K.-H. Song, M. Zhou, S. Jin, G. Zhang, H.-B. Yao, *J. Am. Chem. Soc.*, 2021, **143**, 10860-10864.
- 62 J. Chen, X. Pan, X. Zhang, C. Sun, C. Chen, X. Ji, R. Chen, L. Mao, *Small*, 2023, **19**, 2300938.

View Article Online
DOI: 10.1039/D4NR02262A

